Electronic Supplementary Material (ESI) for Sustainable Energy & Fuels.

Supporting Information

Highly porous Ti-Ni anodes for electrochemical oxidations

Nihal Guenani,[1] Mariam Barawi,[2] Ignacio J. Villar-García, [2] Juan Bisquert,[1]
Víctor A. de la Peña O´Shea[2*] and Antonio Guerrero[1*]

[1] Institute of Advanced Materials (INAM), Universitat Jaume I, 12006 Castelló, Spain.
[2] Photoactivated processes Unit. IMDEA Energy Institute, Avda. Ramón de la Sagra, 3, 28937, Mostoles, Madrid, Spain.

Email: victor.delapenya@imdea.org, *aguerrer@uji.es*
14 May 2020

1. Methods

Materials

All materials were used as received: micrometer size Ni powder (<150µm, Sigma Aldrich 99.99%), Ni nm powder (<100 nm, Sigma Aldrich 99%), Ti powder (100 mesh, Sigma Aldrich, 99.7%), DSA based on Ir (DeNora), flat Ni sheet (ElectroCell).

Film and Device characterization

The Scanning electron microscopy measurements were carried out in a JEOL 7001F equipment operating at 15 kV. The X-ray powder diffraction (XRD) analysis were recorded by means of a BRUKER D4 Endeavor diffractometer using Cu-Kα radiation. XPS spectra were recorded using a SPECS NAP-XPS System incorporating the DeviSim NAP reaction cell. The spectrometer is equipped with a Al Kα monochromated source (hν = 1486.6 eV), composed of a SPECS XR50 MF x-ray gun and a µ-FOCUS 600 monochromator, and PHOIBOS 150 NAP 1D-DLD analyser. X-ray gun power was set to 25 W (1.68 mA emission current and 15 kV). With this X-ray settings, the intensity of the Ag $3d_{5/2}$ photoemission peak for a Ag sample, recorded at 10 eV pass energy (PE), was 1×10^4 cps and the full width at half maximum (FWHM) was 0.60 eV. Binding energy calibration was made using Au $4f_{7/2}$ (84.01 eV), Ag $3d_{5/2}$ (368.20 eV) and Cu $2p_{3/2}$ (932.55 eV). The survey scans were acquired using 30 eV pass energy, 1 eV step size and 7 seconds (1 s x 7 scans) dwell times. Ti 2p and Ni 2p high resolution spectra were acquired using 10 eV pass energy, 0.1 eV step size and 30 seconds (1s x 30 scans) dwell times. The sample was analysed at an electron take-off angle normal to the surface with respect to the analyser.

Electrochemical measurements

The electrochemical measurements were performed in a three-electrode glass cell containing an aqueous solution. Current density and voltage dependence were measured with a potentiostat-galvanostat PGSTAT302N. Impedance Spectroscopy measurements were completed in OER conditions to measure the electrode capacitance to estimate the surface area of the green compact.

OER: Green compact samples were used as working electrode in a 1M NaOH solution with Pt wire counter electrode and Ag/AgCl as reference electrode. Before the measurements, the solution was bubbled with N_2 for 5 minutes. J-V curves and chronoamperometry measurements were recorded and the products formation was measured by in-line gas chromatography as described in supplementary material. In order to quantify the generated products, the cell was connected to a gas chromatograph (Agilent micro-GC 490), equipped with a molecular sieve (MS5) column and a TCD detector, has been used, taking a sample of the gas every *ca.* 3 min.

2. Porosity of electrodes

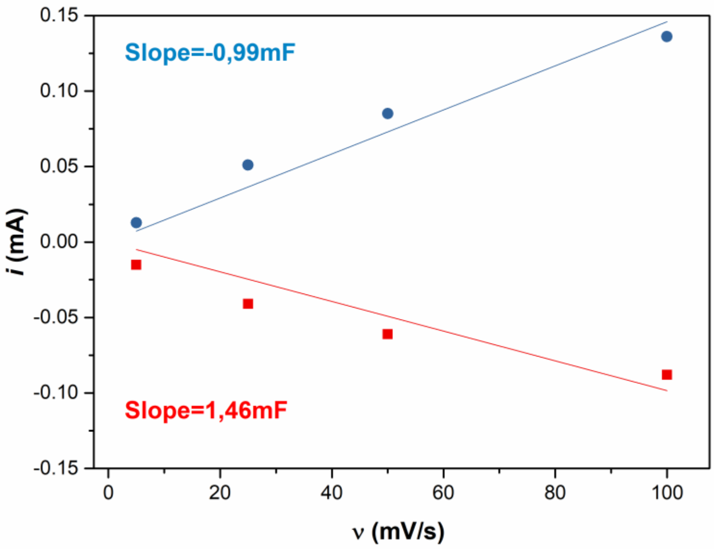

Figure SI1: Current *vs* scan rate linear fit obtained from cyclic voltammetry measurements at different scan rates centered at open circuit voltage of a Ni20 sample with Ag/AgCl and Pt used as reference and counter electrode, respectively.[1]

3. Optimization Oxygen Evolution Reaction (OER)

A whole set of experiments to optimize the performance of the electrodes has been carried out such as modification of the sintering temperatures and times, the particle size or modification of the pH. The sintering time can be reduced by increasing the temperature. Figure SI1 shows green compact electrodes performance as a function of the sintering temperature for reduced sintering times. In this experiment, temperatures of 700 ºC enables the reduction of sintering time by half to obtain similar performance.

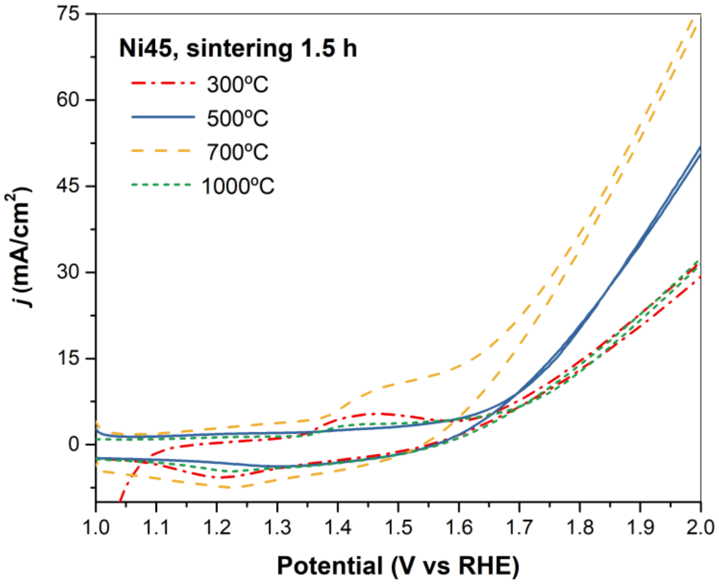

Figure SI2: Current density-voltage curves of Ni45 electrodes sintered at different temperatures over a period of 1.5 h.

In addition, the size of the powders is very important to provide efficient electrodes as shown in Figure SI2 and despite it may be expected that the use of nanoparticle size Ni powder will increase the surface area, and the number of catalytic sites, the observed trend is just the opposite. Indeed, we observed that blending a coarser fraction of Ti with a nanoparticle size fraction of Ni fills the interstices between large Ti particles and during the sintering process, the nanoparticles preferentially coalesce to form large aggregates. Similarly, if the Ti powder is considerably larger (mm size) the porosity is significantly reduced in line with the performance.

Table SI1: Reported best materials performance and comparison with our current work for the OER.

Electrode	**Overpotential at 1 mA/cm^2/ V vs RHE**	**Overpotential at 10 mA/cm^2 V vs RHE**	***iR* Compensated**	**Ref**
NiFe/MoNi$_4$	~170	NA (masked by additional oxidation peak)	No	2
NiFe	200	250	No	3
CrNN+NiFe LDH	230	270	Yes	4
TiNi	250	270-300	No	Our work
IrO$_2$	270	430	Yes	5
RuO$_2$	220	300-440	Yes	5
G-FeCoW	240	315	-	6
CoS$_2$	270	308	-	7

3.1 Faradaic efficiency for OER.

The Faradaic efficiency (FE) of the OER of products was calculated as:

$$FE(\%) = \frac{niF\ \phi iFm}{I\,A\,t} \qquad (1)$$

where ni is the number of the electrons needed for the electrochemical reaction, F is the Faraday constant, ϕi is the volume fraction of the gases, I is the current obtained and Fm is the molar carrier gas gas flow rate. The number of electrons associated with formation of H_2 and O_2 1 electrons and 2 electrons, respectively. The volume fraction of the gases is calculated by calibrating the gas chromatogram (GC) using a diluted mixture of gases of known concentrations.

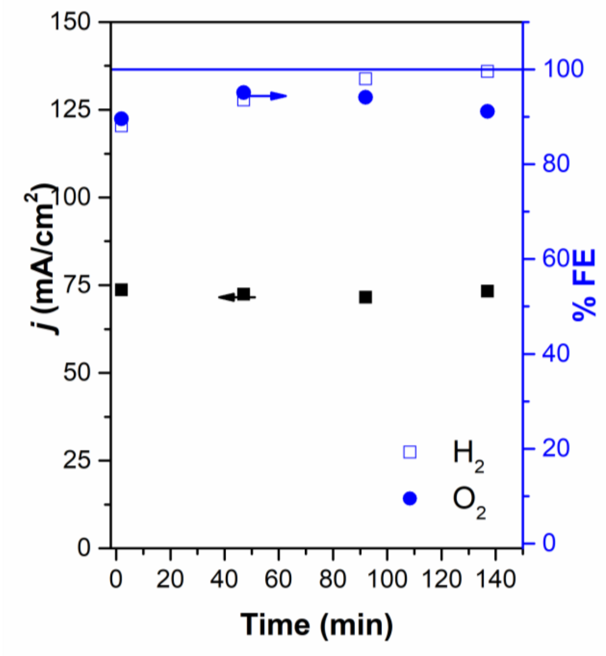

Figure SI3: Chronoamperometry and Faradaic Efficiency calculation for H_2 and O_2 formation using Ni45 as working electrode, Pt as counter electrode and Ag/Ag$^+$ as reference at 1.8 V (vs RHE).

References

1. C. C. L. McCrory, S. Jung, J. C. Peters and T. F. Jaramillo, *J. Am. Chem. Soc.*, 2013, **135**, 16977-16987.
2. H. Zhou, F. Yu, Q. Zhu, J. Sun, F. Qin, L. Yu, J. Bao, Y. Yu, S. Chen and Z. Ren, *Energy Environ. Sci.*, 2018, **11**, 2858-2864.
3. X. Lu and C. Zhao, *Nature Communications*, 2015, **6**, 6616.
4. M. Gong, W. Zhou, M. J. Kenney, R. Kapusta, S. Cowley, Y. Wu, B. Lu, M.-C. Lin, D.-Y. Wang, J. Yang, B.-J. Hwang and H. Dai, *Angewandte Chemie International Edition*, 2015, **54**, 11989-11993.
5. Y. Lee, J. Suntivich, K. J. May, E. E. Perry and Y. Shao-Horn, *J. Phys. Chem. Lett.*, 2012, **3**, 399-404.
6. B. Zhang, X. Zheng, O. Voznyy, R. Comin, M. Bajdich, M. García-Melchor, L. Han, J. Xu, M. Liu, L. Zheng, F. P. García de Arquer, C. T. Dinh, F. Fan, M. Yuan, E. Yassitepe, N. Chen, T. Regier, P. Liu, Y. Li, P. De Luna, A. Janmohamed, H. L. Xin, H. Yang, A. Vojvodic and E. H. Sargent, *Science*, 2016, **352**, 333-337.
7. Y. Hua, H. Jiang, H. Jiang, H. Zhang and C. Li, *Electrochim. Acta*, 2018, **278**, 219-225.